Clays and Clay Minerals, Vol. 59, No. 2, 116–135, 2011.

SURFACE AREA AND POROSITY OF NANOTUBES OBTAINED FROM KAOLIN MINERALS OF DIFFERENT STRUCTURAL ORDER

JAKUB MATUSIK[1,*], EWA WISŁA-WALSH[2], ADAM GAWEŁ[1], ELŻBIETA BIELAŃSKA[3], AND KRZYSZTOF BAHRANOWSKI[1]

[1] AGH University of Science and Technology; Faculty of Geology, Geophysics and Environmental Protection, al. Mickiewicza 30, 30-059 Krakow, Poland
[2]AGH University of Science and Technology, Faculty of Mechanical Engineering and Robotics, Krakow, Poland
[3] Institute of Catalysis and Surface Chemistry, Polish Academy of Sciences, Krakow, Poland

Abstract—Mesoporous materials with pore diameters in the range 2−50 nm forming tubular or fibrous structures are of great interest due to their unique properties. Because they are commonly used as sorbents and catalyst carriers, knowledge of their surface area and porosity is critical. A modified intercalation/deintercalation method was used to increase the efficiency of nanotube formation from kaolin-group minerals which differ in terms of their degree of structural order. Unlike previous experiments, in the procedure adopted in the present study, methanol was used instead of 1,3-butanediol for grafting reactions and octadecylamine intercalation was also performed. The samples were examined using X-ray diffraction (XRD), Fourier-transform infrared spectroscopy (FTIR), differential scanning calorimetry (DSC), and transmission electron microscopy (TEM). The specific surface area and porosity of previously described and newly formed materials were investigated by N_2 adsorption/desorption. Compared to results described earlier, the percent yield of nanotubes obtained in the present study was significantly greater only in the case of 'Maria III' kaolinite, which has high structural order. This increase was obtained mainly by the grafting reaction with methanol. Highly ordered stacking of kaolinite-methanol intercalates was noticed and, thus, the amine intercalation was more efficient. In particular, the use of long-chain octadecylamine significantly increased the nanotube yield. The grafting reaction with methanol procedure yielded fewer nanotubes, however, when applied to poorly ordered samples ('Jaroszów' kaolinite and 'Dunino' halloysite). In the case of the 'Maria III' kaolinite, the diameter of the rolled layers observed by TEM was ~30 nm and corresponded to average diameters of newly formed pores (D_mN) determined using N_2 adsorption/desorption, confirming that nanotubes contributed to an increase in surface area and total pore volume. In the case of 'Jaroszów' kaolinite and 'Dunino' halloysite mainly macropores (D_mN > 100 nm) and mesopores (20 nm > D_mN > 40 nm) were formed. The pores were attributed to interparticle and interaggregate spaces in the stacks of platy particles and to the small relative number of nanotubes.

Key Words—Halloysite, Kaolinite, Nanotubes, Nitrogen Sorption, Porosity.

INTRODUCTION

Mesoporous materials are an important group of porous structures used as sorbents and catalyst supports in processes which involve the use of organic macromolecules (Lu and Zhao, 2004; Burness, 2009). Several template methods have been developed for their synthesis which led to formation of materials such as MCM-41, SBA-15, and FSM-16 (Inagaki *et al.*, 1993; Lin and Mou, 1996; Zhao *et al.*, 1998). The dimensions and shape of mesopores which show highly ordered arrangement can be controlled effectively by changing the synthesis procedure. The advantages of mesoporous silicas are mainly their large surface areas and thermal stability. Internal as well as external surfaces of such tubular derivatives are susceptible to chemical modification by means of active molecules. Lee *et al.* (2009) demonstrated the possibility of loading gold nanoparticles on several types of mesoporous structures. Such molecular sieves were also reported to be capable of binding catalytically active metalloporphyrin molecules. The metalloporphyrin obtained supported heterogenous catalysts with interesting properties (Połtowicz *et al.*, 2001, 2006, 2009; Zimowska *et al.*, 2007). Materials like this were also produced using relatively cheap, naturally occurring clays such as kaolin-group minerals (Nakagaki *et al.*, 2006; Madhusoodana *et al.*, 2006; Nakagaki and Wypych, 2007; Machado *et al.*, 2008).

Kaolinite is an aluminum silicate characterized by a layered 1:1 dioctahedral structure with the chemical composition $Al_2Si_2O_5(OH)_4$. Kaolin-group minerals which include kaolinite, dickite, nacrite, and halloysite (hydrated phase) are polytypes built from identical 1:1 layers but stacked in different ways (*e.g.* Kogure and Inoue, 2005; Brigatti *et al.*, 2006). Kaolinite is the most abundant clay mineral, with a world production of ~20 million tons/year (Murray, 2000; Harvey and Lagaly, 2006). Kaolinite exhibits platy morphology but has been shown to be susceptible to transformation to

* E-mail address of corresponding author:
jakub_matusik@wp.pl
DOI: 10.1346/CCMN.2011.0590202

nanosized tubes by means of intercalation/deintercalation methods (Gardolinski and Lagaly, 2005; Matusik *et al.*, 2009). Worth emphasizing is that the kaolin mineral structure is preserved during the intercalation/deintercalation process. The nanotubes formed possess two chemically different surfaces, *i.e.* the internal surface with aluminol groups of the octahedral sheet and the external surface made up of silica rings of the tetrahedral sheet (Singh, 1996; Singh and Mackinnon, 1996). A decrease in hydrogen-bond strength, assumed to be induced by intercalation and subsequent deintercalation of the long-chain amine, led to the rolling of kaolinite layers. However, the number of nanotubes observed by TEM was relatively small and was attributed to inefficient experimental steps such as grafting with 1,3-butanediol (Matusik *et al.*, 2009).

In the present study, kaolin-group minerals of different structural order were subjected to a modified intercalation/deintercalation method in order to increase the number of nanotubes formed. In contrast to previous experiments (Matusik *et al.*, 2009), methanol was used for the grafting reaction instead of diol, and the minerals were intercalated with octadecylamine instead of hexylamine. The delamination efficiency and structural changes in the minerals subjected to this experimental procedure were then studied. To the best of the authors' knowledge, this is the first time N_2 adsorption/ desorption measurements were performed to investigate the surface area and porosity of the previously obtained (Matusik *et al.*, 2009) and newly formed nanotubular materials.

MATERIALS AND METHODS

Materials

Samples of kaolin-group minerals differing in degree of structural order were obtained from the following Polish deposits: 'Maria III' (well crystallized kaolinite) – M, 'Jaroszów' (poorly crystallized kaolinite) – J, and 'Dunino' (halloysite and kaolinite mixture) – H. The <2 μm fraction was separated by centrifugation and used for all reactions. In addition, a <40 μm fraction of kaolin from the 'Maria III' deposit – M40, was used. Dimethyl sulfoxide (DMSO), methanol, diethyl ether, and toluene were obtained from POCH (Polish Chemical Reagents). Hexylamine and octadecylamine were purchased from Merck (Germany).

Experimental procedure

Synthesis consisted of successive experimental stages which were performed for all starting materials. First, intercalates of minerals with dimethyl sulfoxide (DMSO) were prepared by dispersing 2 g of mineral in a mixture of 27 mL of DMSO and 3 mL of H_2O. The dispersion was heated to 70ºC by means of microwave radiation for 2 h (Zhang and Xu, 2007). The sample was then centrifuged and dried at 60ºC for 24 h (KDS). Second, the precursors obtained were reacted with methanol in order to synthesize grafted derivatives (KM) (Komori *et al.*, 1998, 1999). The DMSO complexes were stirred at room temperature with methanol for 24 h. The centrifuged product was then dispersed in a fresh portion of methanol and this step was repeated seven times. Third, the wet KM methanol-grafted compounds were subjected to intercalation reactions with hexylamine (KMHX) (Gardolinski and Lagaly, 2005). Fourth, hexylamine was exchanged with octadecylamine by reacting wet KMHX mineral-hexylamine compounds with melted octadecylamine (~80ºC) under constant stirring for 72 h (KMOD). Finally, the centrifuged and dried hexylamine (KMHX) and octadecylamine (KMOD) derivatives were subjected to deintercalation reactions with the use of toluene and ultrasound treatment (Gardolinski and Lagaly, 2005). The final products, KHT and KMOT, were dried at 60ºC for 24 h. The preparation of KT (toluene deintercalated hexylamine complexes previously grafted with 1,3-butanediol) derivatives for which the surface area and porosity were also examined has been described elsewhere (Matusik *et al.*, 2009).

Analytical methods

Powder X-ray diffraction (XRD) patterns were recorded using a Philips APD PW 3020 X'Pert instrument with CuKα radiation and a graphite diffracted-beam monochromator. Randomly oriented samples were analyzed in the range 2 to 30º2θ with a step size of 0.05º2θ. The degree of intercalation (ID) was estimated only on the basis of the 001 peak intensities of the raw kaolinite (I_{7R}) and the kaolinite after intercalation (I_7), according to the formula ID = 100% – (I_7/I_{7R})*100% (Matusik *et al.*, 2009). *WinFit* 1.2.1 software (Krumm, 1996) was used for decomposition of the diffraction peaks in the 20–23º2θ region, which was necessary for the Aparicio-Galán-Ferrell index (AGFI) calculations (Aparicio *et al.*, 2006). The Scherrer formula was used to calculate the average number of layers per crystallite from the 002 reflection broadening (Patterson, 1939).

The FTIR spectra were collected using a Bio-Rad FTS-60 spectrometer (Hercules, California, USA) from standard KBr pellets (sample/KBr mass ratio: 1/200 mg) with 256 scans at 2 cm^{-1} resolution in the region 4000–400 cm^{-1}.

A Netzsch STA 409 PC/PG spectrometer (Selb, Germany) was used to record differential scanning calorimetric (DSC) and thermogravimetric (TG) curves. The measurements were performed using 10 mg samples and a temperature range of 25–1000ºC, with a heating rate of 10ºC/min and an air flow of 30 mL/min.

The particle-size distribution, in the range from 0.02 to 2000 μm, was determined by a laser diffraction method by means of a Mastersizer 2000 (Malvern, UK) instrument.

Specific surface area and porosity were determined from N_2 adsorption/desorption isotherms. Sorption

experiments were performed at 77 K using a QUANTACHROME Autosorb-1 spectrometer (Boynton Beach, Florida, USA) in the relative pressure range ~$5.8 \times 10^{-6} < P/P_0 <$ ~0.9959 (sample mass: ~100 mg). Prior to measurements, the samples were outgassed at 423 K. The BET equation and the t method (Lippens and de Boer *et al.*, 1965) were used for surface-area calculations (S^{BET}, S^{t}) (Brunauer *et al.*, 1938; Bahranowski *et al.*, 2000). The total pore volume (V^{tot}) was calculated from the amount of N_2 adsorbed at a relative vapor pressure (P/P_0) close to 1.0. The volume of micropores ($V^{t}_{\mu p}$) was calculated by applying the t method (Lippens and de Boer *et al.*, 1965). In addition, the Dubinin-Radushkevich method was used to estimate the volume of micropores (W^{DR}_{o}) (Dubinin, 1960). Mesopore volume (V^{D}_{mp}) was determined from the adsorption branch of the isotherms using the BJH (Barrett-Joyner-Halenda) method (Barrett *et al.*, 1951) in the mesopore range proposed by Dubinin (1960). The mesopore volume (V_{mp}) was also calculated by subtracting the micropore volume ($V^{t}_{\mu p}$) from the total pore volume (V^{tot}). In addition, the mean diameter of all pores (D_m) and the mean diameter of the group of newly formed pores (D_mN) were calculated using the following equations:

$$D_m = 4V^{tot}/S^{BET} \quad (1)$$

$$D_m N = 4(V^{tot}P - V^{tot}R)/(S^{BET}P - S^{BET}R) \quad (2)$$

where V^{tot}P and V^{tot}R and S^{BET}P and S^{BET}R denote the total pore volumes and surface areas of the final product and the raw starting material, respectively.

Final-product morphology was determined using a JEOL JSM 7500F field emission scanning electron microscope. The microscope had a built-in TEM mode in which the images were recorded.

RESULTS AND DISCUSSION

Synthesis of nanotubes

The structural properties of the starting materials (M, M40, J, and H samples) were described in detail in a previous study (Matusik *et al.*, 2009). The XRD patterns and FTIR spectra of the minerals after each modification step are described below (Figures 1, 2).

Preparation of DMSO derivatives (KDS). The XRD and FTIR analyses revealed no structural differences between complexes obtained from the reactions when using microwave radiation compared with intercalates obtained previously (Matusik *et al.*, 2009), without microwave radiation. Note, however, that microwave radiation reduced the synthesis time to only 2 h.

A sharp peak was observed at 11.26 Å in the XRD patterns of samples after reaction, which confirmed that DMSO molecules were intercalated (Figure 1; samples MDS, M40DS, JDS, HDS) (Olejnik *et al.*, 1968). The changes in peak intensity and the appearance of new peaks in the 19–23º2θ region, as well as the appearance of second- (5.62 Å) and third- (3.73 Å) order reflections, indicated an increase in stacking order, as reported by Matusik *et al.* (2009).

The calculated intercalation degree (ID) was 98% for the MDS sample, 96% for M40DS, 89% for JDS, and 70% for HDS. The ID values were larger for complexes obtained using microwaves than the ID values from Matusik *et al.* (2009); microwave radiation may have favored the separation of kaolinite particles from non-swelling illite or SiO_2 particles, making the kaolin more accessible for DMSO intercalation (Lee *et al.*, 1975; Zhang and Xu, 2007). A higher reaction temperature (70ºC) also contributed to the intercalation of smectite layers (S-I) present in the J sample, as indicated by a peak at 18.78 Å (Berkheiser and Mortland, 1975) (Figure 1).

An increase in the synthesis time to 6 h failed to increase intercalation degree to 100% confirming that, under the experimental conditions that were applied, the maximum intercalation degree was achieved in the samples studied.

The formation of bonds between DMSO and inner-surface hydroxyls of the clay minerals was confirmed by IR spectroscopy (Figure 2). The OH-stretching vibrations (3600–3000 cm^{-1}) (Farmer and Russell, 1967; Farmer, 1974) were noticeably altered in accordance with earlier findings (Olejnik *et al.*, 1968; Matusik *et al.*, 2009) (Figure 2).

Interlayer grafting with methanol (KM). The reaction of the KDS precursors with methanol led to the formation of new grafted derivatives, as was confirmed by a sharp peak at ~11.12 Å in the XRD patterns of wet samples (Figure 1; samples MM, M40M, JM, and HM). The observed basal spacings were in good agreement with those reported in the literature (Komori *et al.*, 1998, 1999; Gardolinski and Lagaly, 2005). Sharp and symmetric basal reflections of new, grafted derivatives suggested a well defined arrangement of methanol molecules in the clay interlayer space, which was most noticeable in the well ordered 'Maria III' kaolinite samples (MM and M40M). For all KM complexes, a third-order reflection was also observed at ~3.70 Å (Figure 1). The changes in peak position and intensity in the range 19–23º2θ, as well as the lack of second- (5.62 Å) and third- (3.73 Å) order reflections characteristic of DMSO complexes, suggested that the intercalated structure was changed as a result of low-temperature grafting. The low-angle reflection at 16.75 Å in the XRD pattern of the JM sample indicated that the DMSO-smectite complex was also modified after methanol treatment. This probably led to the formation of a smectite-methanol derivative with two layers of methanol in the smectite interlayer space (Brindley and Satyabrata, 1964) (Figure 1).

Calculated values for ID were 92% for the MM sample, 90% for M40, 83% for JM, and 72% for HM. A

comparison of these values with the ID values of KDS complexes suggested that the grafting process affected only layers previously intercalated with DMSO. The layers which were unchanged in the reaction with DMSO were unaltered by the reaction with methanol; moreover, earlier reports asserted that the intercalation of raw kaolinite with methanol is impossible (Komori *et al.*, 1998, 1999).

The presence of interlayer methanol after drying was also confirmed by changes in the IR spectra (Figure 2). In the OH-stretching region (3800−3600 cm^{-1}) the band at ~3660 cm^{-1} disappeared and the relative intensity of the band at ~3696 cm^{-1} decreased in comparison to the spectra of the raw samples, and a new band at ~3550 cm^{-1} was observed. This is evidence that inner-surface hydroxyls reacted with the methanol molecules (Tunney and Detellier, 1996). In turn, the high intensity of the band at ~3622 cm^{-1} indicated that inner structural hydroxyls, present inside the layer, probably did not take part in the reaction. In the C−H stretching region (3000−2800 cm^{-1}), new bands with relatively low intensities appeared at ~2930 and ~2846 cm^{-1}, which are characteristic of aluminum methoxide (Guertin *et al.*, 1956) and confirmed the presence of methoxide species in the kaolinite interlayer space (Tunney and Detellier, 1996). The removal of DMSO molecules was confirmed by the disappearance of bands at ~3540 and ~3503 cm^{-1} which corresponded to bonds between DMSO molecules and inner-surface hydroxyls.

Alcohol complexes remain stable only when stored in liquid methanol. Air drying, therefore, led to a rapid destruction of the new complex with d_{001} = 11.12 Å. The process failed to remove the methanol completely, however. Drying at room temperature resulted in the formation of a stable complex with $d_{001} \approx 9.0$ Å (data not shown).

Hexylamine and octadecylamine intercalation (KMHX; KMOD). The intercalation of hexylamine and the formation of new derivatives were observed for all samples, as indicated by the appearance of a basal spacing of 26.3 Å in the XRD patterns (Figure 1; samples: MMHX, M40MHX, JMHX, HMHX). The d_{001} value was in good agreement with values reported in the literature and suggested a perpendicular arrangement of amine chains with respect to kaolinite layers (Komori *et al.*, 1999; Gardolinski and Lagaly, 2005). A symmetric basal peak indicated a well defined arrangement of hexylamine molecules in the interlayer space and was particularly noticeable in samples containing minerals of high structural order (MMHX and M40MHX) (Figure 1). A sharp reflection at 20.0 Å in XRD patterns of hexylamine complexes was related to the crystalline product of hexylamine oxidation. Clear differences in the 6−11°2θ range were observed between MMHX, M40MHX, JMHX, and HMHX samples (Figure 1). In the case of MMHX and M40MHX samples, a broad reflection with marked peak at 11.45 Å, due to interlayer methanol molecules, was observed (Gardolinski and Lagaly, 2005). In turn, for JMHX and HMHX samples, second- (12.96 Å) and third- (8.66 Å) order reflections of a 26.3 Å basal spacing were also observed. A peak at ~11.12 Å for sample HMHX indicated that some layers still contained methanol as observed in sample HM. For all samples the third-order reflection at 3.70 Å disappeared (Figure 1). Unchanged kaolinite layers were also still present after reaction, as attested by the peak at ~7.2 Å.

The amino groups of interlayer hexylamine molecules formed hydrogen bonds with the mineral surfaces, as confirmed by a broad IR band with two maxima at ~3434 and ~3523 cm^{-1} (Komori *et al.*, 1999) (Figure 2). In addition, three bands appeared at ~2900 cm^{-1} which may be related to C−H stretching vibrations of the amine aliphatic chain.

After reaction with the kaolin, crystalline octadecylamine is difficult to remove by washing because of the possibility of destroying the KMOD intercalate. Structural characterization of a mixture of KMOD intercalate with crystalline octadecylamine was, therefore, necessary in order to assess the extent of complex formation. The XRD patterns after reaction revealed new peaks which were assigned to the formation of octadecylamine complex: 58.6 Å (basal spacing of new octadecylamine complex) and 28.6 Å (second-order reflection; samples: MMOD, M40MOD, JMOD, and HMOD). The d_{001} value was similar to those reported previously, at 57.5 Å (Komori *et al.*, 1999) and 53.2 Å (Gardolinski and Lagaly, 2005) and confirmed a perpendicular arrangement of octadecylamine chains as for hexylamine. In addition, a number of reflections was observed which can be attributed to the crystalline octadecylamine (Figure 1).

In the IR spectra, bands related to crystalline octadecylamine as well as the amine present in the interlayer space appeared (Figure 2). The bands attributed to the formation of mineral−amine hydrogen bonds were marked in the 3600−3200 cm^{-1} region, while C−H stretching vibrations were present in the 3000−2800 cm^{-1} range (Komori *et al.*, 1999; Gardolinski and Lagaly, 2005). The bands with very low intensities in the OH-stretching region characteristic of the kaolin minerals were also noted (Figure 2).

Deintercalation of amine-intercalated minerals (KHT; KMOT). The hexylamine and octadecylamine molecules were completely removed from the interlayer space of amine intercalates as indicated by the disappearance of low-angle basal reflections at 26.3 Å (KHT samples) and 58.6 Å (KMOT samples) in the XRD patterns (Figure 1). In the case of MHT, M40HT, MMOT, and M40MOT samples, a broad peak in the 6−11°2θ range was noted at ~8.7 Å (Figure 1).

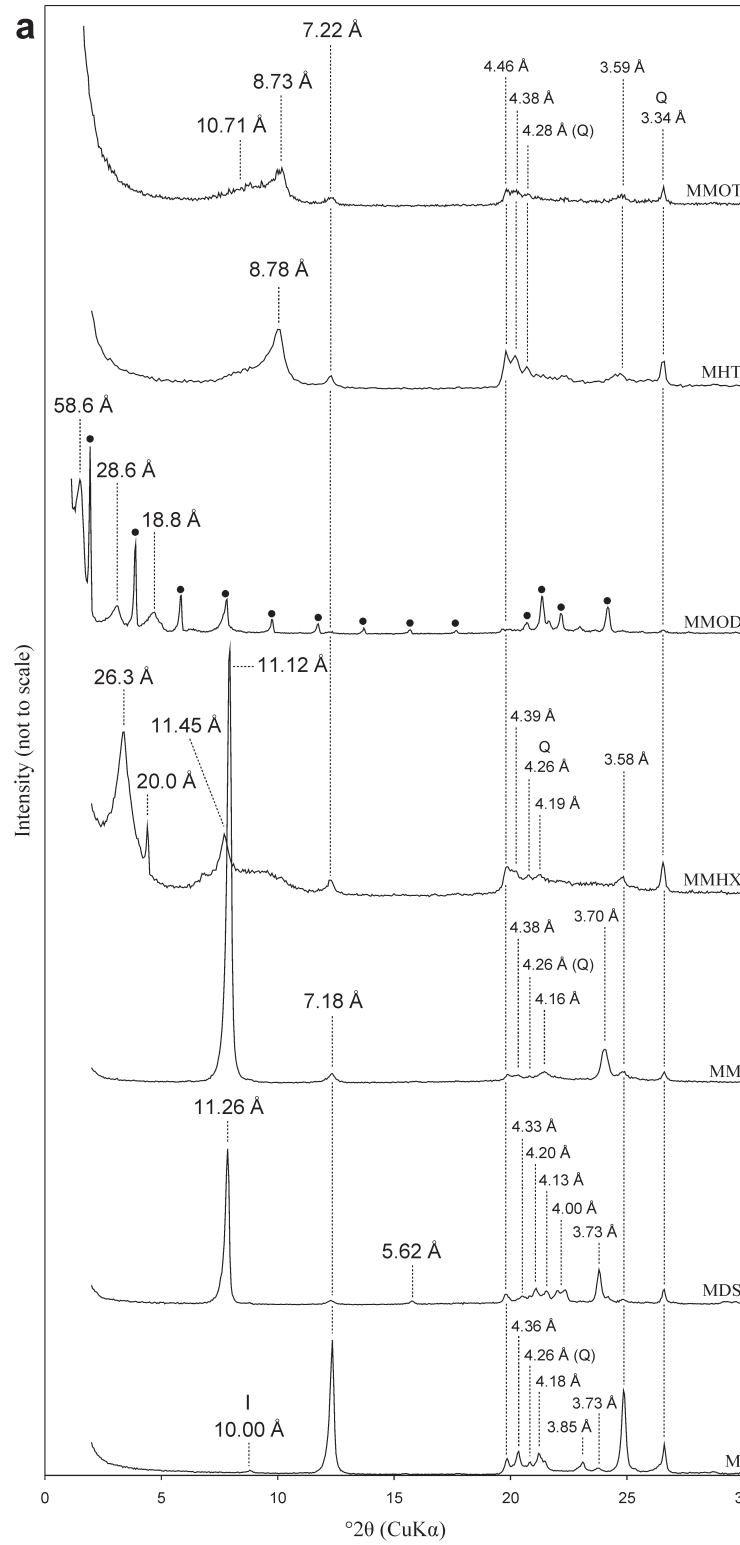

Figure 1 (*this and following three pages*). XRD patterns of: (a) M – 'Maria III' kaolinite (<2 μm), (b) M40 – 'Maria III' kaolinite (<40 μm), (c) J – 'Jaroszów' kaolinite (<2 μm), (d) H – 'Dunino' halloysite (<2 μm) after: DS – DMSO intercalation, M – methanol grafting, MHX – hexylamine intercalation, MOD – octadecylamine intercalation, HT – deintercalation of KMHX intercalates by toluene, and MOT – deintercalation of KMOD intercalates by toluene. Abbreviations: Q – quartz, I – illite, S-I – mixed-layer smectite-illite, ● – peaks of crystalline octadecylamine.

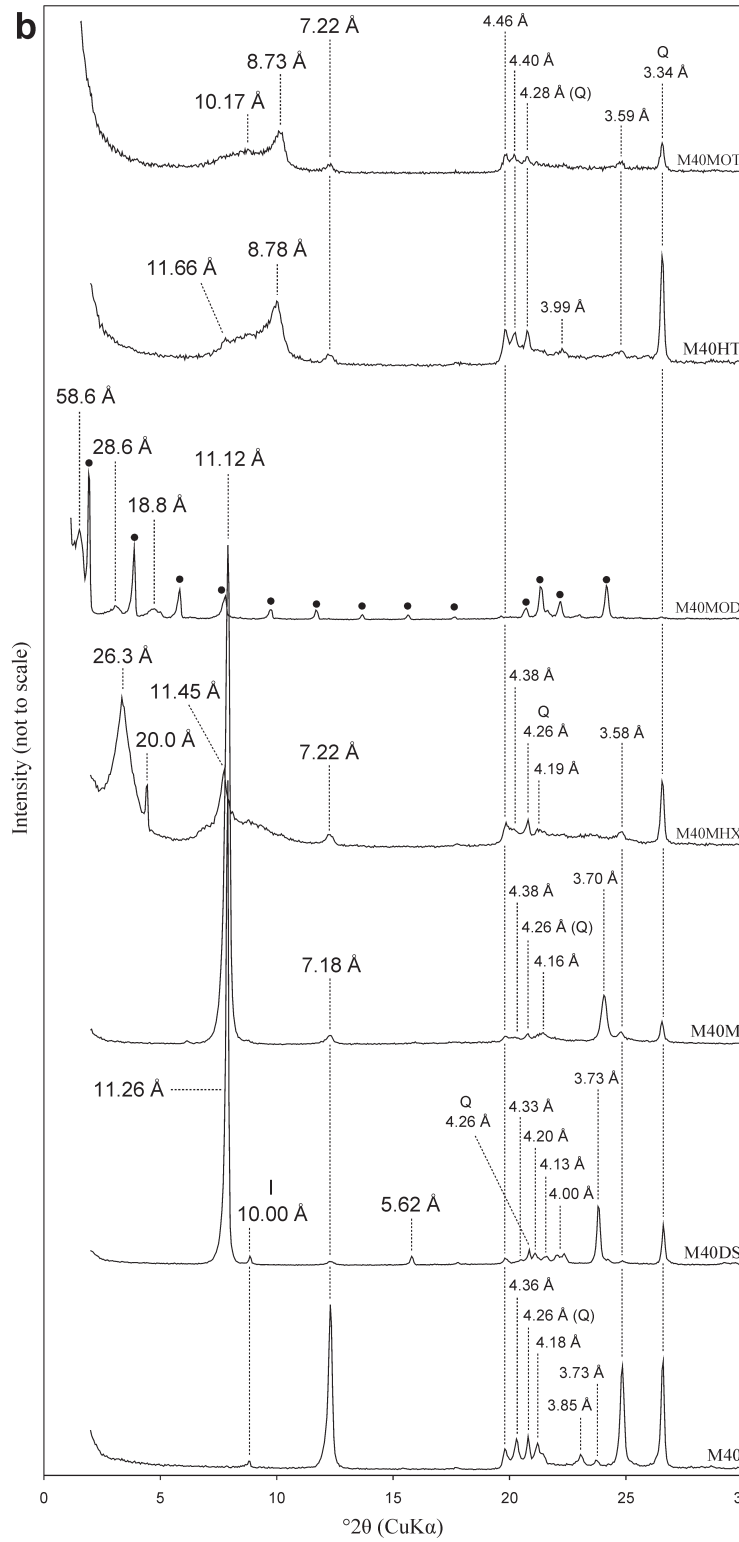

On the other hand, in the case of samples containing minerals with low structural order, a broad reflection was observed in the 6–11º2θ range with less noticeable maxima at: 9.13 Å (JHT), 9.25 Å (HHT), 10.05 Å and 8.77 Å (JMOT), and 10.98 Å (HMOT). The peaks may indicate the presence of a dried mineral-methanol complex (Komori *et al.*, 1998).

The IR spectra of deintercalated KHT samples

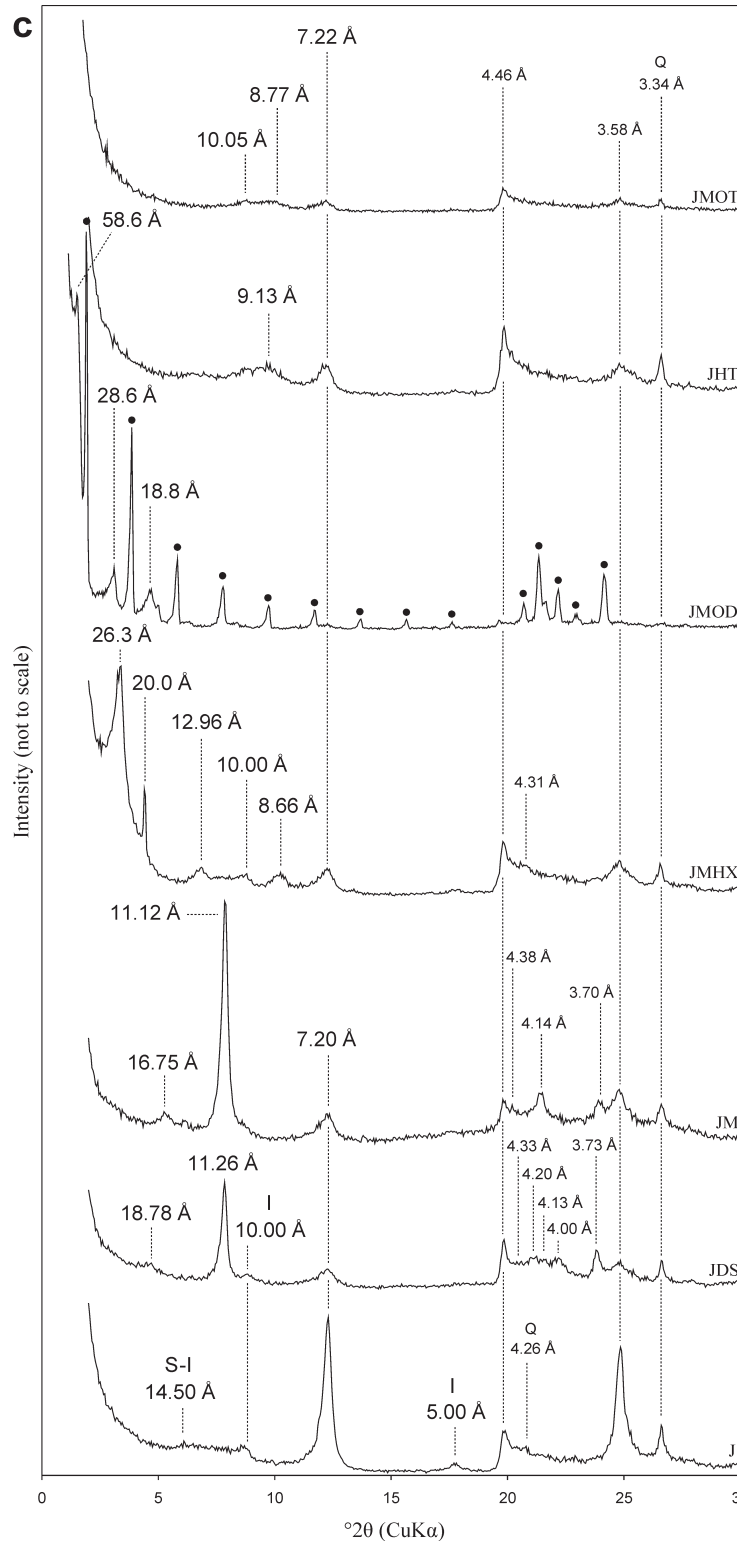

showed no evidence of changes compared with the spectra for KMHX samples (Figure 2). A broad band in the 3600−3300 cm^{-1} range was noted for the KHT and KMOT samples, indicating that organic amine chains were still bonded to the mineral surface. For KMOT samples a significant decrease in bands attributed to crystalline octadecylamine was observed, which confirmed its partial removal (Figure 2).

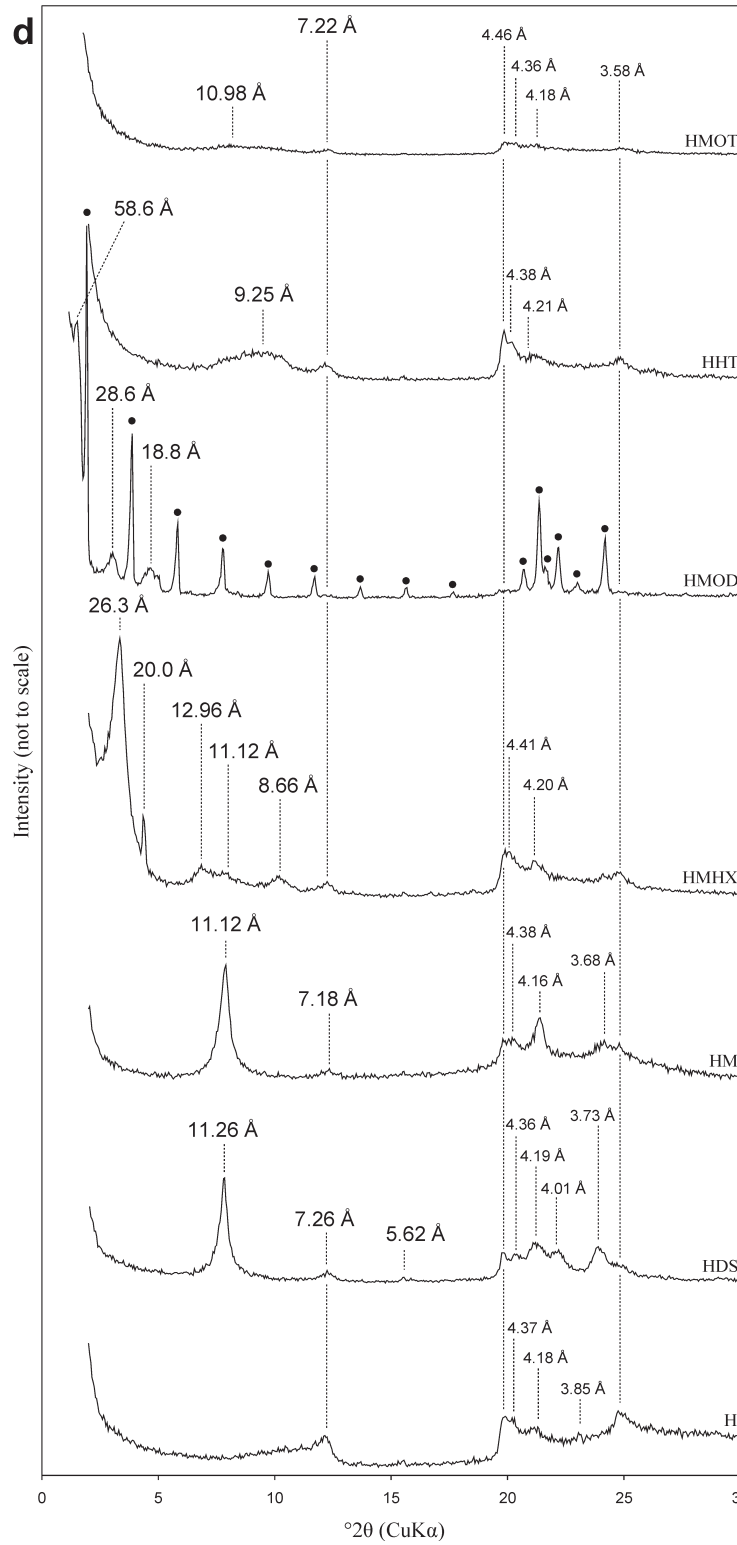

The DSC curves recorded for the KT, KHT, and KMOT samples showed effects characteristic of raw minerals of the kaolin group: dehydroxylation near 500ºC and structural reorganization followed by the synthesis of mullite-type phases at >950ºC (Figure 3). Exothermic peaks were also observed in the 300–350ºC range, however, which can be attributed to the removal of amine molecules and some covalently bonded

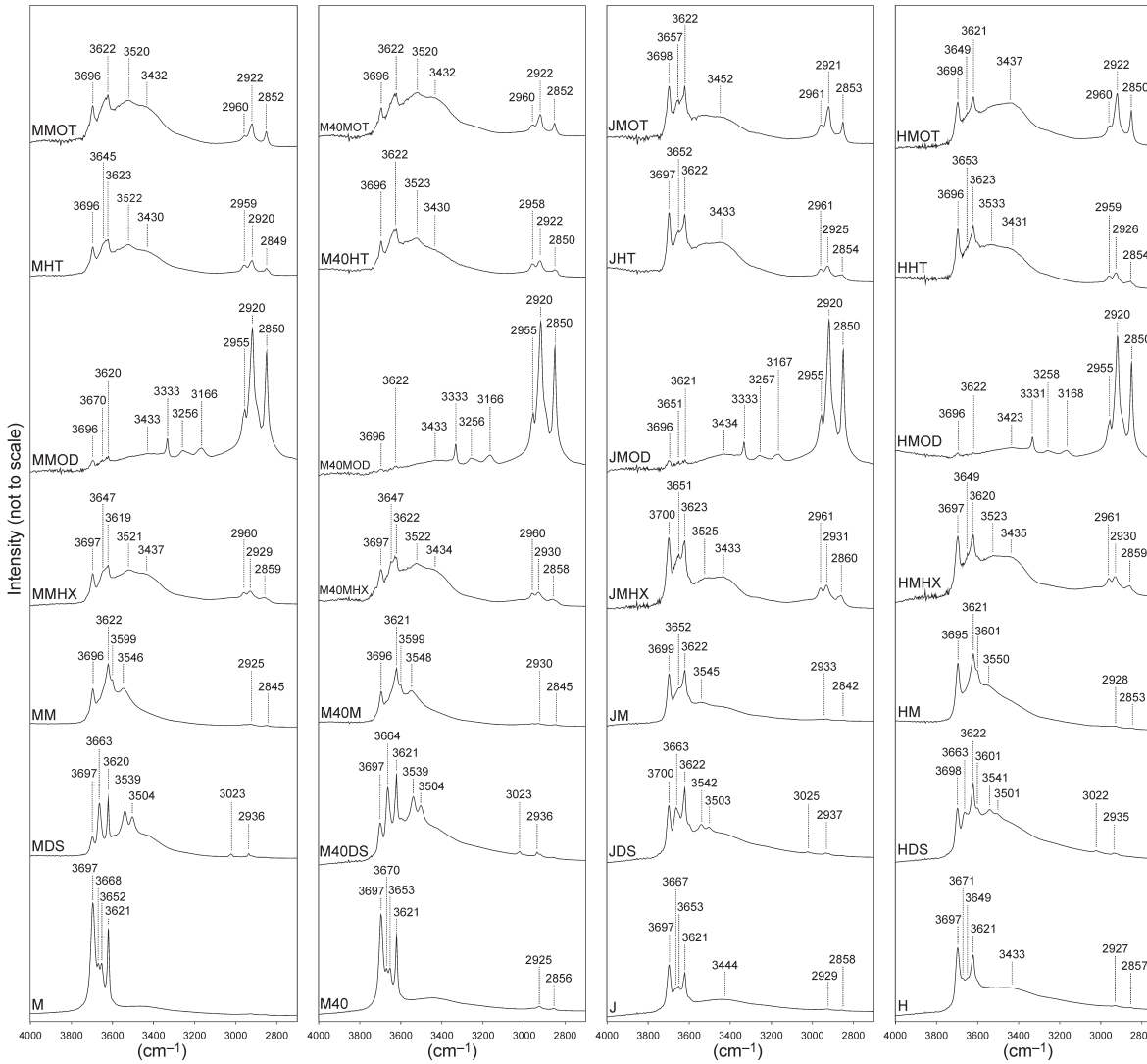

Figure 2. FTIR spectra in the 4000–2700 cm^{-1} region of: M – 'Maria III' kaolinite (<2 μm), M40 – 'Maria III' kaolinite (<40 μm), J – 'Jaroszów' kaolinite (<2 μm), and H – 'Dunino' halloysite (<2 μm). Sample nomenclature as for Figure 1.

methanol molecules (Figure 3). For all derivatives, a shift in the dehydroxylation peak position toward lower temperatures compared with the raw samples was observed, possibly suggesting a reduction in particle size and/or a modification in the stacking sequences in the mineral (Figure 3).

Delamination and structural changes in kaolin minerals

The applied procedure caused a remarkable delamination of 'Maria III' kaolinite particles (Figure 4). Regardless of size fraction (M and M40 samples), the mean number of layers forming coherent scattering domains decreased from ~160 (raw sample) to ~30 (final products). The clearest decrease was noted after the first two experimental steps. Samples containing minerals of low structural order (J and H) were not delaminated to a significant extent. For the J sample, the mean number of layers decreased from ~40 to ~20, while in the case of the H sample it stayed at the same level of ~20.

The structural order changes were estimated using the AGFI, taking into consideration the limitations of the method described earlier (Matusik *et al.*, 2009). The experimental procedure led to a significant decrease in structural order in the case of the M and M40 samples (Figure 5). A decrease in structural order was observed in samples J and H after deintercalation of the hexylamine complexes (KHT) (Figure 5). The JMOT and HMOT products showed slightly greater structural order compared with the pristine J and H samples (Figure 5). The AGFI values of methanol-grafted compounds were not taken into account as the XRD patterns were recorded using wet samples.

Examination of surface area and porosity

Raw samples. Particle-size distribution curves were bimodal, except for the M40 sample, with peaks at 0.18 μm and 4.36 μm (M and H sample), and 0.14 μm and 0.72 μm (J sample) (Figure 6). The laser-diffraction method characterizes the particle size with the assumption that all particles are spheres. Kaolin-group minerals mainly form platy particles. The mean values of peaks which resulted from the measurement may, therefore, correspond to the true dimensions of the particles and may also be related to the existence of several groups of particles which differ in size (Heffels *et al.*, 1996; Xu and Guida, 2003).

The largest particle size was observed for the M40 sample, where the median was equal to 7.58 μm. The median values of the M and H samples were very similar to one another at 2.02 μm and 2.42 μm, respectively. The J sample consisted of the smallest particles with a median size of 0.14 μm. The parameters presented correlated well with the values of cumulative surface (S_{CUM}), values which ignore grain porosity. The greatest S_{CUM} value of 19.00 m^2/g was observed in sample J, with the smallest particles, and the smallest value of 0.44 m^2/g was observed in sample M40, with the largest particles. The S_{CUM} values for M and H samples were 7.88 m^2/g and 6.87 m^2/g, respectively.

Isotherms of the raw samples were of type II with hysteresis loop H3 (Figures 7, 9, 10, 12), corresponding to a mesoporous character with the formation of slit-shaped pores arising from the stacking of platy particles (Sing *et al.*, 1985; Rouquerol *et al.*, 1998). The hysteresis loops for the J and H samples had no closure points, while in the case of the M and M40 samples the closure points were lower than usually observed for N_2 adsorption at P/P_o = 0.36 and 0.08, respectively. This may be related to irreversible uptake of N_2 molecules in pores of about the same width as that of the adsorbate (Sing *et al.*, 1985).

Calculated adsorption parameters of the starting materials clearly differed (Table 1). The H sample had the greatest surface area (S^{BET}) and total pore volume (V^{tot}) among the starting materials, 63.46 m^2/g and 0.2624 cm^3/g, respectively (Table 1). The surface area of the H sample reflected primarily its mesoporosity, but a small fraction of micropores was also observed. The J sample also showed relatively large S^{BET} and V^{tot} values, 41.11 m^2/g and 0.1950 cm^3/g, respectively. These values were significantly smaller for the M and M40 samples. In none of the samples did S^{BET} and V^{tot} exceed 12.35 m^2/g and ~0.11 cm^3/g, respectively. The S^{BET} and V^{tot} values were greater for minerals with lower structural order due to the smaller particle size, as observed in samples J and H (Figure 6), which is a result of defect accumulation (Meunier, 2006) (Figure 5).

Comparing the S_{CUM} values with the S^{BET} values is interesting (Table 1). The closest agreement between them was observed in the case of the M sample, suggesting that the porosity of its grains was very low. Although the H sample had an S_{CUM} value very similar to that of the M sample, its S^{BET} value was five times greater, indicating the presence of highly porous grains. The differences between S_{CUM} and S_{BET} values in the cases of the J and H samples, compared with the M samples, suggested a different internal structure of grains for these samples, a possible effect of different mineral composition in these samples. Kaolinite was the dominant mineral in the J sample while the H sample was derived mainly from halloysite. For sample M40, the presence of relatively large grains led to a decrease in the S_{CUM} value.

V^{tot} of raw samples was in the range of mesopore volumes (V^{D}_{mp}). This observation, as well as the mean pore diameter (D_m), confirmed a mesoporous character for raw samples.

Data calculated using the t method revealed that a small portion of micropores ($V^{t}_{\mu p}$) was present in all raw samples. In turn, the micropore volumes obtained using the Dubinin-Radushkevich method (W^{DR}_{o}) indicated the greatest values in J and H samples. Differences between micropore volumes calculated by the t and Dubinin-Radushkevich methods ($V^{t}_{\mu p}$ and W^{DR}_{o}) were the result of different regions of micropores being considered by these two methods (Wisła, 1982).

Derivatives of 'Maria III' kaolinite (<2 μm) – MT, MHT, MMOT. The experimental steps T, HT, and MOT had no effect on the type of isotherm obtained from the M sample (Figure 7). The adsorption isotherms were of type II with hysteresis loops of the H3 type (Sing *et al.*, 1985; Rouquerol *et al.*, 1998), which are characteristic for mesoporous materials. The width and closure point of the hysteresis loop depended on the type of experimental procedure applied. Hysteresis-loop widths increased consecutively for samples MT, MHT, and MMOT. No loop-closure points were observed in samples MT or MHT, whereas the loop-closure point was observed in sample MMOT at P/P_o = 0.28. The hysteresis loop of H3 type was assigned to mesoporous materials and was observed for aggregates of plate-like particles, giving rise to slit-shaped pores (Sing *et al.*, 1985). The increase in loop width and the fact that closure points were either absent or smaller than usually observed for N_2 (normally observed at P/P_o = 0.42 (Sing *et al.*, 1985)) indicated the formation of pores from which desorption was hindered while reducing the pressure.

In the relative pressure range of $0.03 < P/P_0 < 1.0$, the amount of N_2 uptake followed the sequence M > MT > MHT > MMOT (Table 1). Moreover, the amount of N_2 sorbed at maximum pressure $P/P_0 \approx 0.995$ increased in the same sequence (Table 1), suggesting that the experimental steps caused a gradual increase in both S^{BET} and V^{tot}. The S^{BET} increased from 12.35 m^2/g (M sample) to 20.76 m^2/g (MT sample), to 28.34 m^2/g

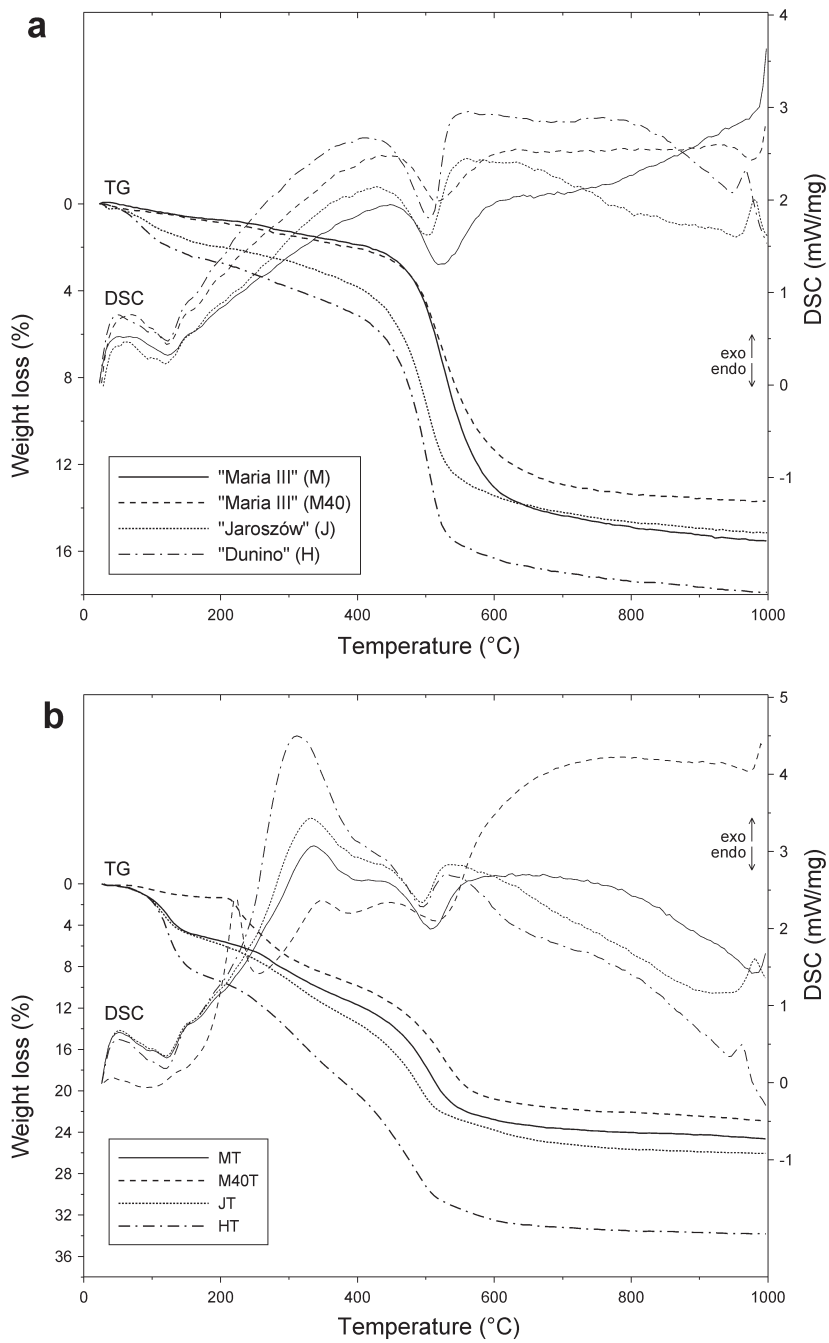

Figure 3 (*this and facing page*). DSC-TG curves: (a) raw samples, (b) KT derivatives, (c) KHT derivatives, (d) KMOT derivatives.

(MHT sample), and to 29.43 m^2/g (MMOT sample). In turn, the V^{tot} increased from 0.1125 cm^3/g (M sample) to 0.1801 cm^3/g (MT sample), to 0.2394 cm^3/g (MHT sample), and to 0.2527 cm^3/g (MMOT sample). The values of V^{tot} were in good agreement with the values of mesopore volumes calculated according to the BJH method, but taking into account the mesopore range proposed by Dubinin (V^{D}_{mp}), confirming that the MT, MHT, and MMOT samples investigated were predominantly mesoporous. The fraction of micropores increased for all derivatives. Such a tendency was in agreement with the values of micropore volumes estimated using the Dubinin-Radushkevich equation. The micropore volume, W_o, changed from 0.0036 cm^3/g for the M sample to 0.0080 cm^3/g (MT sample), 0.0099 cm^3/g (MHT sample), and 0.0159 cm^3/g (MMOT sample). The

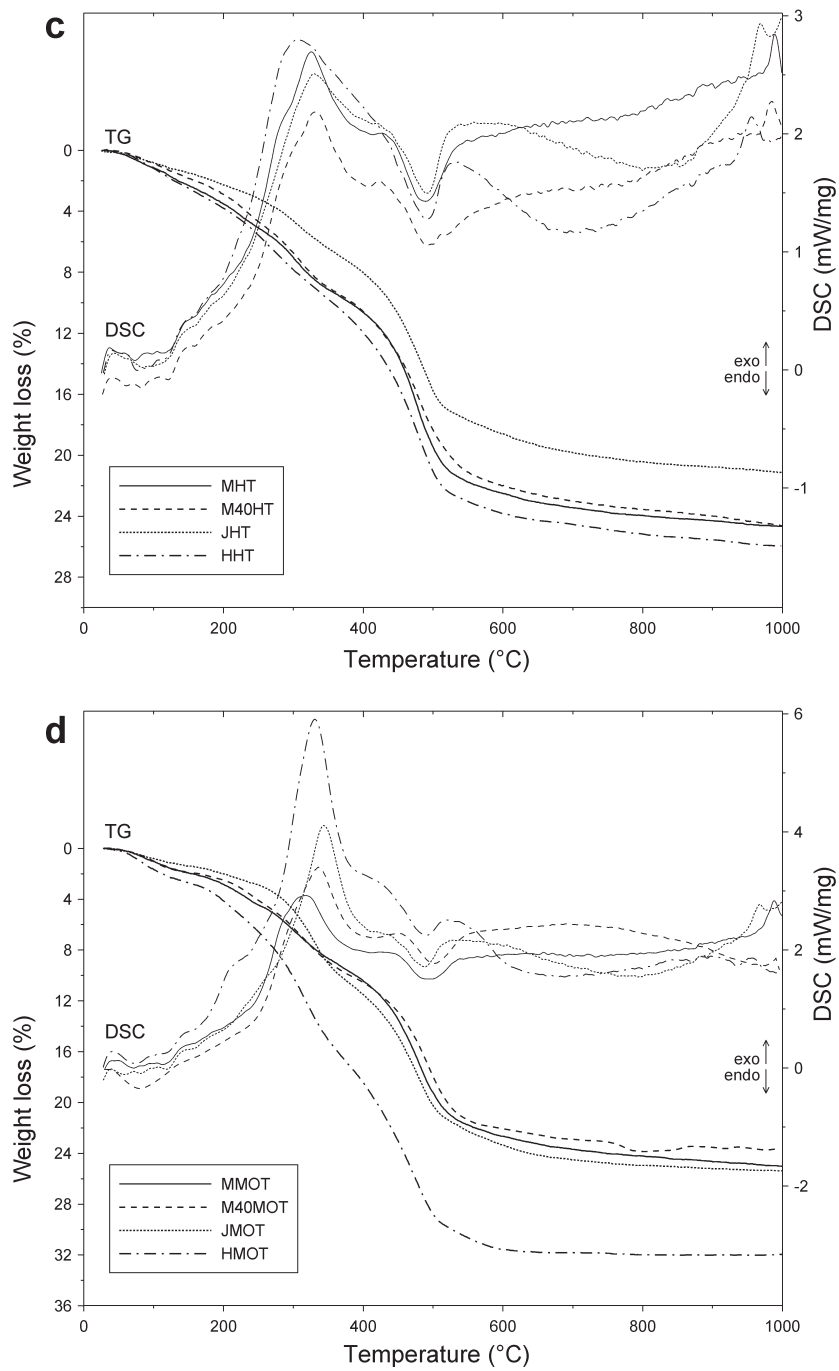

microporosity could be attributed to incomplete removal of organic compounds from the interlayer space of derivatives (Matusik *et al.*, 2009). Taking into account the fact that nanotube formation was expected as a result of the procedures used, the mean diameter of newly formed pores was estimated according to equation 2. The calculated mean diameter D_mN (Table 1) was in very good agreement with the diameters of nanotubes observed by TEM (Figure 8). The mean diameter of the tubes in the TEM images was estimated to be ~30 nm, while their lengths depended on the particle size of the starting material (Matusik *et al.*, 2009). Agreement among the values obtained was clearer in the case of MHT and MMOT samples, where the D_mN values were ~26.0 nm and ~27.3 nm, respectively. This may be related to the largest number of nanotubes being

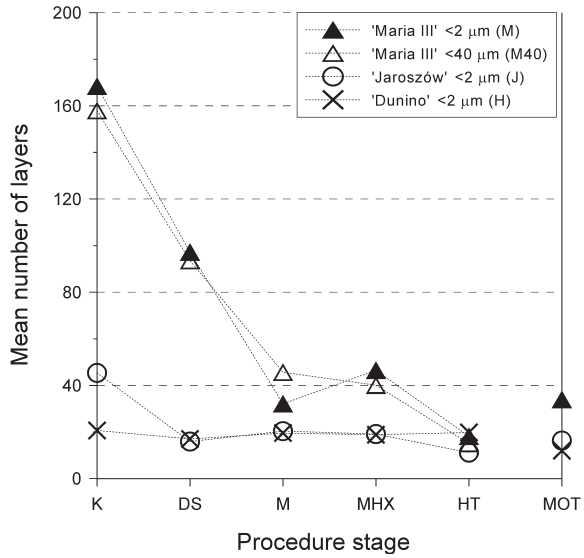

Figure 4. Changes in average number of layers for kaolin-group minerals. Sample nomenclature as in Figure 1.

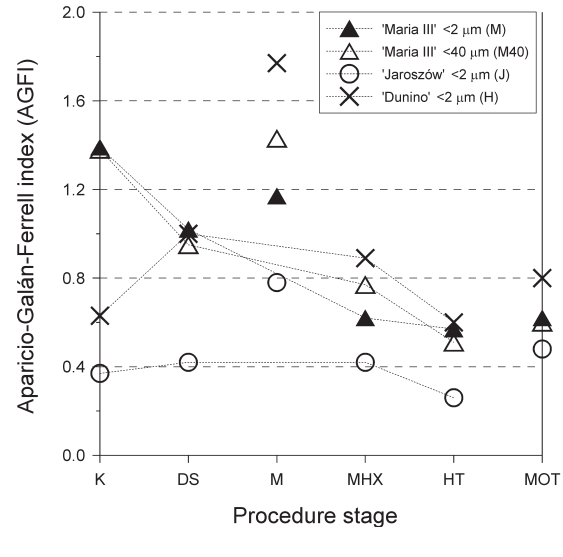

Figure 5. Changes in AGFI for kaolin-group minerals. Sample nomenclature as for Figure 1.

observed for these samples. Lesser agreement was noted for the MT sample, where the rolling processes were less intense (Matusik *et al.*, 2009). The formation of tubes contributed to an increase in both S^{BET} and V^{tot}.

Derivatives of 'Maria III' kaolinite (<40 μm) – M40T, M40HT, M40MOT. The type of isotherms observed for derivatives of the M40 sample was unchanged (Figure 9). The isotherms were of type II with noticeable H3 hysteresis loops. The loop width observed for the M40 and M40T samples was similar, whereas it increased incrementally in the M40HT and M40MOT samples. The closure point for the M40T sample was observed at P/P_o = 0.26, whereas for the M40HT and M40MOT samples it was at P/P_o = 0.08. As reported above, the increase in loop width, as well as the closure points being at lower relative pressure than P/P_o = 0.42, were consistent with the appearance of pores from which desorption was hindered.

In contrast with derivatives of the M sample, the amount of N_2 sorbed in the range $0.03 < P/P_0 < 1.0$ for materials obtained from the M40 sample increased in the order M40T < M40 < M40HT < M40MOT (Table 1), whereas at maximum relative pressure the sorption

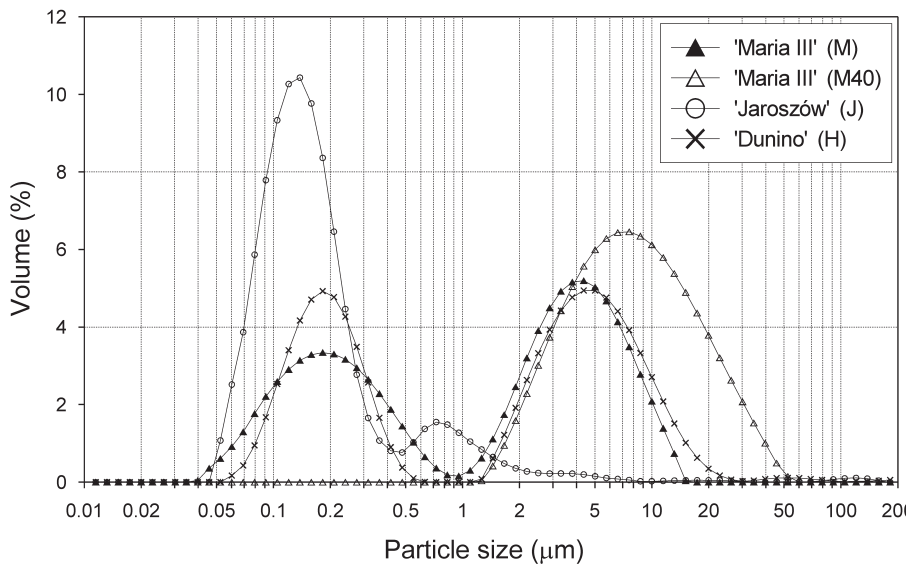

Figure 6. Particle-size distribution of raw samples.

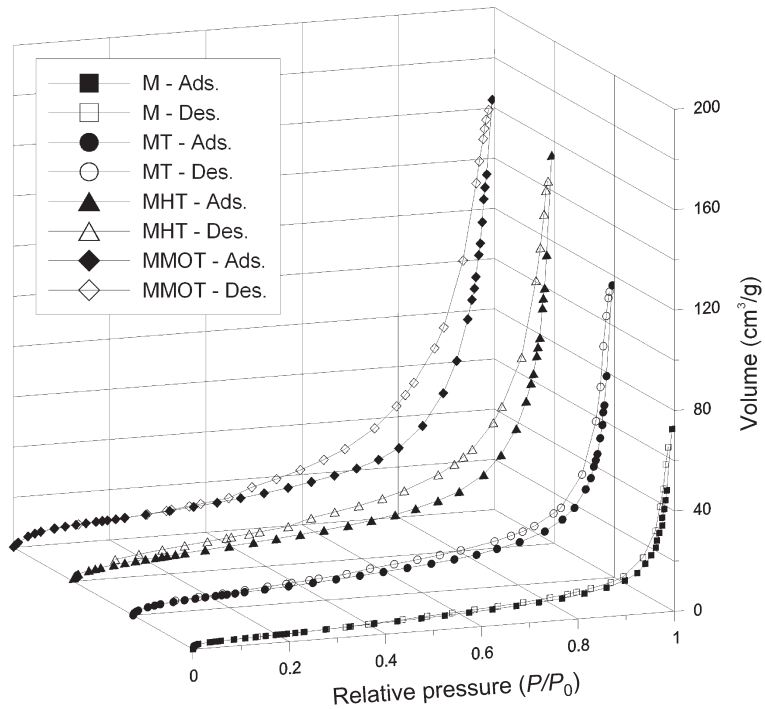

Figure 7. N_2 adsorption/desorption isotherms at 77 K for the 'Maria III' kaolinite (<2 μm) (M) and its derivatives MT, MHT, and MMOT.

increased in the order M40T < M40 < M40MOT < M40HT (Table 1), suggesting that KHT and KMOT procedures caused an increase in S^{BET} and V^{tot} and the KT procedure applied to the M40 sample probably led to the formation of macropores.

The observed increases in S^{BET} and V^{tot} were less in the M40 derivatives compared with the same derivatives obtained from the <2 μm fraction of the 'Maria III' kaolinite. The initial S^{BET} for the M40 sample was 9.74 m^2/g and increased to 22.28 m^2/g for the M40HT sample and to 22.10 m^2/g for the M40MOT sample. The values for V^{tot} for the M40HT and M40MOT samples increased, from the initial value of 0.1183 cm^3/g in the M40 sample to 0.1970 cm^3/g and 0.1788 cm^3/g, respectively. For sample M40T, a decrease in S^{BET} to 4.08 m^2/g was observed, as well as a slight decrease in V^{tot} to 0.0948 cm^3/g.

Mesopores were still the dominant group of pores for all derivatives, as confirmed by the good agreement between the values of V^{tot} and V^{D}_{mp}. The mean diameters

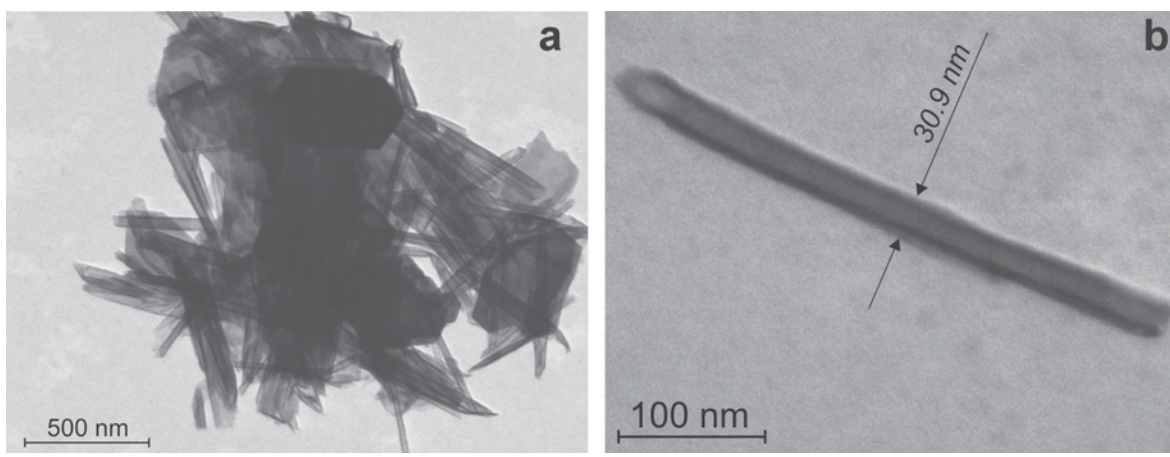

Figure 8. TEM images of 'Maria III' kaolinite derivatives KHT (a) and KMOT (b).

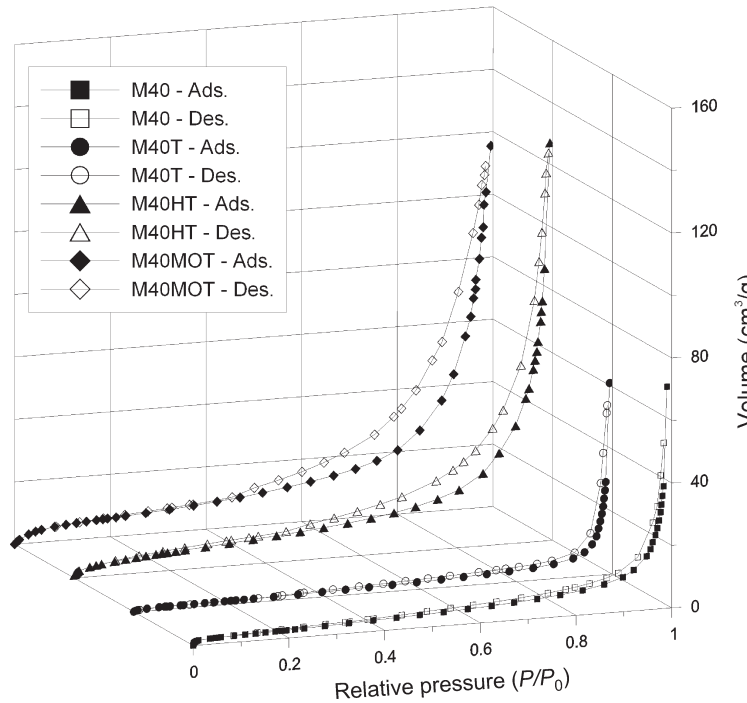

Figure 9. N_2 adsorption/desorption isotherms at 77 K for the 'Maria III' kaolinite (<40 μm) (M40) and its derivatives M40T, M40HT, and M40MOT.

of all pores, D_m, indicated the presence of macropores in the M40T sample.

The W_o^{DR} values suggested an increase in micropore volume to 0.0081 cm^3/g and 0.0119 cm^3/g for the

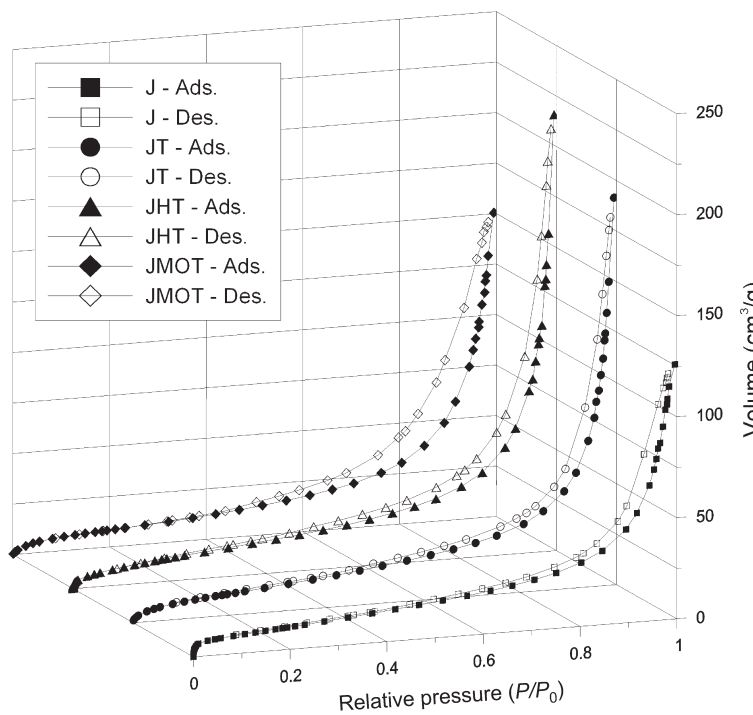

Figure 10. N_2 adsorption/desorption isotherms at 77 K for the 'Jaroszów' kaolinite (<2 μm) (J) and its derivatives JT, JHT, and JMOT.

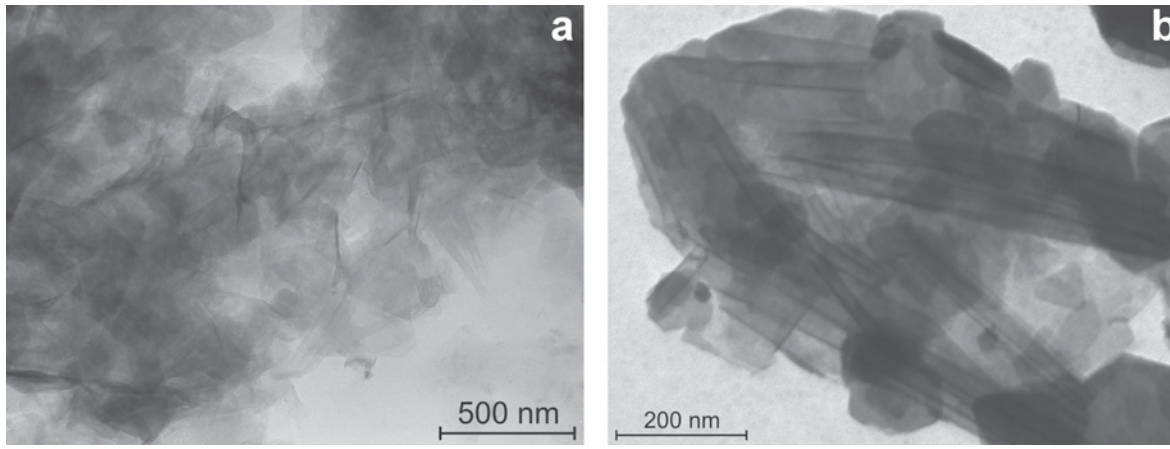

Figure 11. TEM images of 'Jaroszów' kaolinite derivatives JHT (a) and JMOT (b).

M40HT and M40MOT samples, respectively, whereas the micropore volume of the M40T sample decreased.

The diameter of newly formed pores, D_mN, calculated according to equation 2 for M40HT (34.0 nm) and M40MOT (27.2 nm), corresponded to the mean diameter of tubes measured using TEM (Figure 8). Lack of correlation in the case of the M40T sample (D_mN = 8.6 nm) resulted from the formation of only a very small number of nanotubes and confirmed the formation of pores with diameters different from those characteristic of nanotubes.

Derivatives of 'Jaroszów' kaolinite (<2 μm) – JT, JHT, JMOT. The adsorption/desorption isotherms measured for the J sample derivatives JT, JHT, and JMOT were of type II and displayed hysteresis loops of the H3 type (Figure 10). No closure point was present in the hysteresis loop of sample JT, whereas one was present at relative pressures of P/P_0 = 0.10 and 0.27 in samples JHT and JMOT, respectively. The width of the loop for the samples increased in the order J < JT < JHT < JMOT. The isotherms showed very similar gas uptake with increasing pressure; however, above a relative pressure

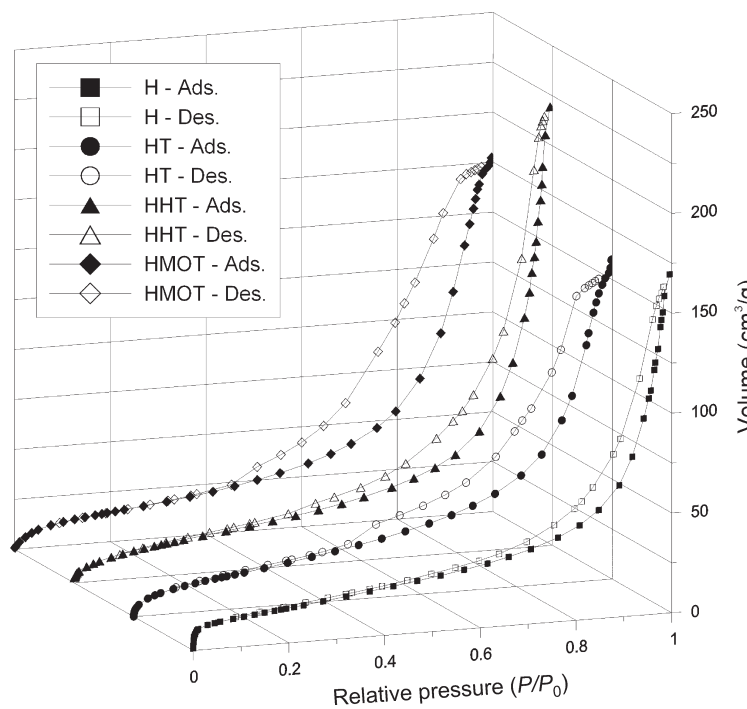

Figure 12. N_2 adsorption/desorption isotherms at 77 K for the 'Dunino' halloysite (<2 μm) (H) and its derivatives HT, HHT, and HMOT.

Table 1. Surface area and porosity parameters calculated for the raw samples and KT, KHT, and KMOT derivatives. Sample nomenclature and parameters abbreviations shown in the Materials and Methods section.

Sample	S^{BET} (m^2/g)	S^{t} (m^2/g)	V^{tot} (cm^3/g)	W_o^{DR} (cm^3/g)	$V^{t}_{\mu p}$ (cm^3/g)	V_{mp} (cm^3/g)	V^{D}_{mp} (cm^3/g)	D_m (nm)	D_mN (nm)	Hysteresis loop	Isotherm type
M	12.35	11.50	0.1125	0.0036	2.91×10^{-5}	0.1125	0.0925	36.4	n.d.	H3	II
MT	20.76	17.72	0.1801	0.0080	b.d.	0.1801	0.1514	34.7	22.4	H3	II
MHT	28.34	26.28	0.2394	0.0099	b.d.	0.2394	0.2408	33.8	26.0	H3	II
MMOT	29.43	28.09	0.2527	0.0159	0.0004	0.2523	0.2333	34.3	27.3	H3	II
M40	9.74	9.11	0.1183	0.0045	3.44×10^{-5}	0.1183	0.1181	48.6	n.d.	H3	II
M40T	4.08	3.73	0.0948	0.0019	b.d.	0.0948	0.0923	92.9	8.6	H3	II
M40HT	22.28	20.53	0.1970	0.0081	b.d.	0.1970	0.1977	35.4	34.0	H3	II
M40MOT	22.10	20.94	0.1788	0.0119	b.d.	0.1788	0.1702	32.4	27.2	H3	II
J	41.11	38.55	0.1950	0.0158	0.0001	0.1949	0.1823	18.9	n.d.	H3	II
JT	41.42	34.05	0.2873	0.0015	b.d.	0.2873	0.2630	27.7	1190	H3	II
JHT	45.11	44.32	0.3341	0.0135	b.d.	0.3341	0.1514	29.6	139	H3	II
JMOT	31.57	29.58	0.2328	0.0153	b.d.	0.2328	0.2031	29.5	15.8	H3	II
H	63.46	62.20	0.2624	0.0243	3.23×10^{-5}	0.2624	0.2448	16.5	n.d.	H3	II
HT	65.56	59.15	0.2412	0.0277	b.d.	0.2412	0.2338	14.7	40.4	H2	II / IV
HHT	63.27	60.08	0.3400	0.0199	b.d.	0.3400	0.3272	21.5	1633	H3	II
HMOT	55.98	51.91	0.2711	0.0259	b.d.	0.2711	0.2765	19.4	4.6	H2	II / IV

b.d. – below detection; n.d. – not determined

of $P/P_0 = 0.95$, the amount of N_2 sorbed increased in the order J < JMOT < JT < JHT (Table 1).

The KT procedure applied in the case of sample J did not affect its S^{BET}; the KHT procedure increased the S^{BET} by 4 m^2/g, and the KMOT procedure led to a decrease in the S^{BET} by 9.54 m^2/g compared with sample J. Even though S^{BET} did not increase, the values of V^{tot} did increase from 0.1950 cm^3/g for starting sample J to 0.2873 cm^3/g for the JT sample, more clearly to 0.3341 cm^3/g for the JHT sample, and to 0.2328 cm^3/g for the JMOT sample. The fraction of micropores, W_o^{DR}, did not change clearly, as indicated by observed values for the JHT and JMOT samples; however, it decreased by a factor of 10 in the case of the JT sample. Taking this into account, the increase in V^{tot} is proposed to be a consequence of the formation of large mesopores and macropores. The mean diameter calculated for all pores (D_m) increased by ~53% for all samples (JT, JHT, and JMOT); however, this result cannot be attributed to the formation of nanotubes, due to the small number of tubes seen in the TEM images (Figure 11). Size comparison of newly formed pores (D_mN) supports the assumption that mainly macropores were formed (Table 1). The observed diameters of newly formed pores differed from diameters measured for the mineral nanotubes (Table 1). The V^{D}_{mp} and W_0^{DR} values were clearly smaller than the V^{tot} values. It must, therefore, be emphasized that the formation of macropores mainly contributed to the increase in V^{tot}, while the S^{BET} decreased or remained unchanged. The observed macropores formed interparticle and interaggregate spaces, resulting from the stacking of individual mineral plates as well as small numbers of tubular particles (Figure 11).

Derivatives of 'Dunino' halloysite (<2 μm) – HT, HHT, HMOT. The adsorption/desorption isotherms obtained for the H sample derivatives revealed a distinct change from type II to a composite of type II and type IV for HT and HMOT samples, along with a change in hysteresis loop to H2 (Figure 12). The HHT sample displayed a type II isotherm with hysteresis loop H3 (Figure 12). The loops of the HT, HHT, and HMOT samples had closure points at relative pressures of P/P_0 = 0.08, 0.08, and 0.25, respectively. No notable change in S^{BET} for HT and HHT was observed, but a distinct decrease was noticed for the HMOT sample (Table 1), related to a small increase in V^{tot}, while the micropore volume (W_0^{DR}) remained almost the same as for the H sample. In the case of the HMOT sample, the experimental procedure probably reduced the fractions of large mesopores and macropores, which was also suggested by a change in the hysteresis loop type from H3 to H2, also indicating a change in pore shape. On the other hand, a small increase in S^{BET}, related to a decrease in V^{tot} and a mean pore diameter of (D_m), was observed for the HT sample. Such changes were probably due to an increase in micropore volume W_0^{DR} compared with the H sample. The largest increase in V^{tot}, by 0.0776 cm^3/g, was observed for sample HHT. As the micropore volume W_0^{DR} decreased for this sample, the mesopore fraction probably increased.

Calculated mean diameters (D_mN) of newly formed pores indicated a predominance of pores with diameters

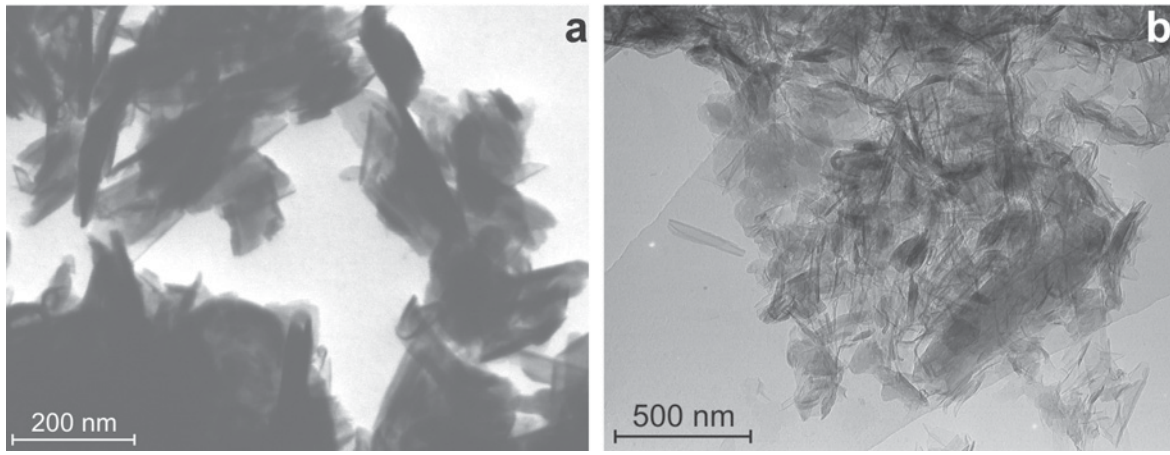

Figure 13. TEM images of 'Dunino' halloysite derivatives HHT (a) and HMOT (b).

different from those observed for nanotubes in the TEM images (Table 1). The pores that formed were, as described above, interparticle and interaggregate, and were classified as macropores (Figure 13). Taking into account the change in hysteresis loop (HT and HMOT samples), the shapes of the pores may have changed from slit-shaped to 'ink bottle'-shaped as a result of the treatment used.

CONCLUSIONS

(1) The modified intercalation/deintercalation procedure led to the formation of nanotubes with diameters of ~30 nm. The number of nanotubes was significantly larger for samples which initially contained minerals of high structural order ('Maria III' kaolinite). In poorly ordered 'Jaroszów' kaolinite and 'Dunino' halloysite the number of rolled layers was very small.

(2) An important role of the grafting process, which determined the efficiency of amine intercalation, was confirmed. The use of methanol rather than 1,3-butanediol, as well as intercalation with octadecylamine, increased the number of nanotubular particles in well ordered 'Maria III' kaolinite.

(3) The applied experimental procedure caused delamination of mineral particles and a decrease in mineral structural order, and was particularly evident in the 'Maria III' kaolinite samples.

(4) N_2 adsorption/desorption experiments revealed the mesoporous character of the materials obtained. All experimental procedures (KT, KHT, and KMOT) led to a significant increase in surface area (S^{BET}) and total pore volume (V^{tot}) for the 'Maria III' kaolinite. The calculated diameters of newly formed groups of pores were in good agreement with those observed by TEM for nanotubes, confirming that the formation of nanotubes contributed to the increase in S^{BET} and V^{tot}.

(5) In the case of 'Jaroszów' kaolinite and 'Dunino' halloysite, the S^{BET} value was not altered noticeably; an increase in V^{tot} was observed, however. For these samples macro- and mesopores were observed in the main, with diameters differing from the diameters of the tubes. These pores formed interparticle and interaggregate spaces which resulted from the stacking of platy particles and nanotubes.

ACKNOWLEDGMENTS

The authors are indebted to Dr J. Sołtys, Managing Director of the 'Intermark' company, for supplying mineral samples from the 'Dunino' deposit. They are also grateful to Drs Roman Dula and Zofia Czuła (Institute of Catalysis and Surface Chemistry, Krakow, Poland) for performing DSC analyses and N_2-sorption experiments, as well as to Dr Łukasz Zych (Faculty of Materials Science and Ceramics, AGH University of Science and Technology) for particle-size measurements. They also thank Professor Bruno Lanson and two anonymous referees for their constructive reviews. This work was supported financially by the Ministry of Science and Higher Education within the research project No. N N307 315336 (2009–2012).

REFERENCES

Aparicio, P., Galán, E., and Ferrell, R.E. (2006) A new kaolinite order index based on XRD profile fitting. *Clay Minerals*, **41**, 811–817.

Bahranowski, K., Kielski, A., Serwicka, E.M., Wisła-Walsh, E., and Wodnicka, K. (2000) Influence of doping with copper on the texture of pillared montmorillonite catalysts. *Microporous and Mesoporous Materials*, **41**, 201–215.

Barrett, E.P., Joyner, L.G., and Halenda, P.P. (1951) The determination of pore volume and area distribution in porous substances. I. Computations from N_2 isotherms. *Journal of the American Chemical Society*, **73**, 373–380.

Berkheiser, V. and Mortland, M.M. (1975) Variability in exchange ion position in smectite: Dependence on interlayer solvent. *Clays and Clay Minerals*, **23**, 404–410.

Brigatti, M.F., Galán, E., Theng, B.K.G., and Lagaly, G. (2006) Structures and mineralogy of clay minerals. Pp. 19–87 in: *Handbook of Clay Science* (F. Bergaya, B.K.G. Theng and G. Lagaly, editors). Developments in Clay Science, Vol. **1**, Elsevier, Amsterdam.

Brindley, G.W. and Satyabrata, R. (1964) Complexes of Ca-

montmorillonite with primary monohydric alcohols (Clay-organic studies-VIII). *American Mineralogist*, **49**, 106–115.

Brunauer, S., Emmett, P.H., and Teller, E. (1938) Adsorption of gases in multimolecular layers. *Journal of the American Chemical Society*, **60**, 309–319.

Burness, L.T. (2009) *Mesoporous Materials: Properties, Preparation and Applications.* Nova Science Publishers, New York.

Dubinin, M.M. (1960) The potential theory of adsorption of gases and vapors for adsorbents with energetically nonuniform surfaces. *Chemical Reviews*, **60**, 235–241.

Farmer, V.C. (1974) The layer silicates. Pp. 331–363 in: *The Infrared Spectra of Minerals* (V.C. Farmer, editor). Monograph **4**, Mineralogical Society, London.

Farmer, V.C. and Russell, J.D. (1967) Infrared absorption spectrometry in clay studies. *Clays and Clay Minerals*, **15**, 121–142.

Gardolinski, J.E.F.C. and Lagaly, G. (2005) Grafted organic derivatives of kaolinite: II. Intercalation of primary n-alkylamines and delamination. *Clay Minerals*, **40**, 547–556.

Guertin, D.L., Wiberly, S.E., Bauer, W.H., and Goldeyson, J. (1956) The infrared spectra of three aluminum alkoxides. *Journal of Physical Chemistry*, **60**, 1018–1019.

Harvey, C.C. and Lagaly, G. (2006) Clays in industry: Conventional application. Pp. 501–541 in: *Handbook of Clay Science* (F. Bergaya, B.K.G. Theng and G. Lagaly, editors). Developments in Clay Science, Vol. **1**, Elsevier, Amsterdam.

Heffels, C.M.G., Verheijen, P.J.T., Heitzmann, D., and Scarlett, B. (1996) Correction of the effect of particle shape on the size distribution measured with a laser diffraction instrument. *Particle & Particle Systems Characterization*, **13**, 271–279.

Inagaki, S., Fukushima, Y., and Kuroda, K. (1993) Synthesis of highly ordered mesoporous materials from a layered polysilicate. *Journal of the Chemical Society, Chemical Communications*, **8**, 680.

Kogure, T. and Inoue, A. (2005) Determination of defect structures in kaolin minerals by high-resolution transmission electron microscopy (HRTEM). *American Mineralogist*, **90**, 85–89.

Komori, Y., Sugahara, Y., and Kuroda, K. (1998) A kaolinite-NMF-methanol intercalation compound as a versatile intermediate for further intercalation reaction of kaolinite. *Journal of Materials Research*, **13**, 930–934.

Komori, Y., Sugahara, Y., and Kuroda, K. (1999) Intercalation of alkylamines and water into kaolinite with methanol kaolinite as intermediate. *Applied Clay Science*, **15**, 241–252.

Krumm, S. (1996) Winfit 1.2: a public domain program for interactive profile-analysis under Windows. *Acta Universitatis Carolinae Geologica*, **38**, 253–261.

Lee, S.Y., Jackson, M.L., and Brown, J.L. (1975) Micaceous occlusions in kaolinite observed by ultramicrotomy and high resolution electron microscopy. *Clays and Clay Minerals*, **23**, 125–129.

Lee, B., Ma, Z., Zhang, Z., Park, C., and Dai, S. (2009) Influences of synthesis conditions and mesoporous structures on the gold nanoparticles supported on mesoporous silica hosts. *Microporous and Mesoporous Materials*, **122**, 160–167.

Lin, H.P. and Mou, C.Y. (1996) "Tubules-Within-a-Tubule" Hierarchical Order of Mesoporous Molecular Sieves in MCM-41. *Science*, **273**, 765.

Lippens, B.C. and de Boer, J.H. (1965) Studies on pore systems in catalysts. V. The t method. *Journal of Catalysis*, **4**, 319–323.

Lu, G.Q. and Zhao, X.S. (2004) *Nanoporous Materials - Science and Engineering*. Imperial College Press, London.

Machado, G.S., Freitas Castro, K.A.D., Wypych, F., and Nakagaki, S. (2008) Immobilization of metalloporphyrins into nanotubes of natural halloysite toward selective catalysts for oxidation reactions. *Journal of Molecular Catalysis A: Chemical*, **283**, 99–107.

Madhusoodana, C.D., Kameshima, Y., Nakajima, A., Okada, K., Kogure, T., and MacKenzie, K.J.D. (2006) Synthesis of high surface Al-containing mesoporous silica from calcined and acid leached kaolinites as the precursors. *Journal of Colloid and Interface Science*, **297**, 724–731.

Matusik, J., Gaweł, A., Bielańska, E., Osuch, W., and Bahranowski, K. (2009) The effect of structural order on nanotubes derived from kaolin-group minerals. *Clays and Clay Minerals*, **57**, 452–464.

Meunier, A. (2006) Why are clay minerals small? *Clay Minerals*, **41**, 551–566.

Murray, H.H. (2000) Traditional and new applications for kaolin, smectite and palygorskite: a general overview. *Applied Clay Science*, **17**, 207–221.

Nakagaki, S. and Wypych, F. (2007) Nanofibrous and nanotubular supports for the immobilization of metalloporphyrins as oxidation catalysts. *Journal of Colloid and Interface Science*, **315**, 142–157.

Nakagaki, S., Machado, G.S., Halma, M., Santos Marangon, A.A., Freitas Castro, K.A.D., Mattoso, N., and Wypych, F. (2006) Immobilization of iron porphyrins in tubular kaolinite obtained by an intercalation/delamination procedure. *Journal of Catalysis*, **242**, 110–117.

Olejnik, J., Aylmore, L.A.G., Posner, A.M., and Quirk, J.P. (1968) Infrared spectra of kaolin mineral-dimethyl sulfoxide complexes. *Journal of Physical Chemistry*, **72**, 241–249.

Patterson, A.L. (1939) The Scherrer formula for X-ray particle size determination. *Physical Review*, **56**, 978–982.

Połtowicz, J., Serwicka, E.M., Bastardo-Gonzales, E., Jones, W., and Mokaya, R. (2001) Oxidation of cyclohexene over Mn(TMPyP) porphyrin-exchanged Al,Si-mesoporous molecular sieves. *Applied Catalysis A: General*, **218**, 211–217.

Połtowicz, J., Pamim, K., Matachowski, L., Serwicka, E.M., Mokaya, R., Xia, Y., and Olejniczak, Z. (2006) Oxidation of cyclooctane over Mn(TMPyP) porphyrin-exchanged Al,Si-mesoporous molecular sieves of MCM-41 and SBA-15 type. *Catalysis Today*, **114**, 287–292.

Połtowicz, J., Bielańska, E., Zimowska, M., Serwicka, E.M., Mokaya, R., and Xia, Y. (2009) Microporosity in mesoporous SBA-15 supports: A factor influencing the catalytic performance of immobilized metalloporphyrin. *Topics in Catalysis*, **52**, 1098–1104.

Rouquérol, J., Rouquérol, F., and Sing, K.S.W. (1998) *Adsorption by Powders & Porous Solids.* Academic Press, London.

Sing, K.S.W., Everett, D.H., Haul, R.A.W., Moscou, L., Pierotti, R.A., Rouquérol, J., and Siemieniewska, T. (1985) Reporting physisorption data for gas/solid systems with special reference to the determination of surface area and porosity. *Pure and Applied Chemistry*, **57**, 603–619.

Singh, B. (1996) Why does halloysite roll? – A new model. *Clays and Clay Minerals*, **44**, 191–196.

Singh, B. and Mackinnon, I.D.R. (1996) Experimental transformation of kaolinite to halloysite. *Clays and Clay Minerals*, **44**, 825–834.

Tunney, J.J. and Detellier, C. (1996) Chemically modified kaolinite. Grafting of methoxy groups on the interlamellar aluminol surface of kaolinite. *Journal of Materials Chemistry*, **6**, 1679–1685.

Wisła, E. (1982) The effect of changes in adsorbent texture on the adsorption of SO_2. PhD thesis, Institute of the Environmental Engineering, Polish Academy of Sciences.

Xu, R. and Di Guida, O.A. (2003) Comparison of sizing small particles using different technologies. *Powder Technology*,

132, 145–153.

Zhang, X. and Xu, Z. (2007) The effect of microwave on preparation of kaolinite/dimethylsulfoxide composite during intercalation process. *Materials Letters*, **61**, 1478–1482.

Zhao, D., Huo, Q., Feng, J., Chmelka, B.F., and Stucky, G.D. (1998) Nonionic triblock and star diblock copolymer and oligomeric surfactant syntheses of highly ordered, hydrothermally stable, mesoporous silica structures. *Journal of the American Chemical Society*, **120**, 6024–6036.

Zimowska, M., Michalik-Zym, A., Połtowicz, J., Bazarnik, M., Bahranowski, K., and Serwicka, E.M. (2007) Catalytic oxidation of cyclohexane over metalloporphyrin supported on mesoporous molecular sieves of FSM-16 type – steric effects induced by nanospace constraints. *Catalysis Today*, **124**, 55–60.

(*Received 6 April 2010; revised 16 March 2011; Ms. 427; A.E. B. Lanson*)